Biochemistry

Article

Cite This: Biochemistry 2018, 57, 4135−4147

pubs.acs.org/biochemistry

Increasing Enzyme Stability and Activity through Hydrogen Bond-Enhanced Halogen Bonds

Anna-Carin C. Carlsson,[†] Matthew R. Scholfield,[†] Rhianon K. Rowe,[†] Melissa Coates Ford,[†] Austin T. Alexander,[‡] Ryan A. Mehl,[‡] and P. Shing Ho*[,†]

[†]Department of Biochemistry & Molecular Biology, Colorado State University, Fort Collins, Colorado 80523, United States

[‡]Department of Biochemistry & Biophysics, Oregon State University, Corvallis, Oregon 97333, United States

Supporting Information

ABSTRACT: The construction of more stable proteins is important in biomolecular engineering, particularly in the design of biologics-based therapeutics. We show here that replacing the tyrosine at position 18 (Y18) of T4 lysozyme with the unnatural amino acid *m*-chlorotyrosine (^{mCl}Y) increases both the thermal stability (increasing the melting temperature by ∼1 °C and the melting enthalpy by 3 kcal/mol) and the enzymatic activity at elevated temperatures (15% higher than that of the parent enzyme at 40 °C) of this classic enzyme. The chlorine of ^{mCl}Y forms a halogen bond (XB) to the carbonyl oxygen of the peptide bond at glycine 28 (G28) in a tight loop near the active site. In this case, the XB potential of the typically weak XB donor Cl is shown from quantum chemical calculations to be significantly enhanced by polarization via an intramolecular hydrogen bond (HB) from the adjacent hydroxyl substituent of the tyrosyl side chain, resulting in a distinctive synergistic HB-enhanced XB (or HeX-B for short) interaction. The larger halogens (bromine and iodine) are not well accommodated within this same loop and, consequently, do not exhibit the effects on protein stability or function associated with the HeX-B interaction. Thus, we have for the first time demonstrated that an XB can be engineered to stabilize and increase the activity of an enzyme, with the increased stabilizing potential of the HeX-B further extending the application of halogenated amino acids in the design of more stable protein therapeutics.

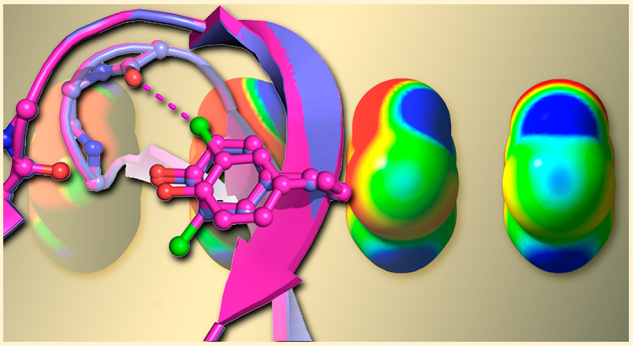

Over the past two decades, recombinant proteins have been developed as biotechnology medicines to treat human diseases; the first such example, insulin, entered clinical trials in 1980 to treat diabetes.[1] Today, the list of approved recombinant therapeutics has grown to include human growth hormone to treat developmental disorders,[2] interferon to control multiple sclerosis and other autoimmune diseases,[3] and erythropoietins to treat anemia associated with kidney disease or chemotherapy,[4] but the numbers remain relatively limited. One of the primary challenges to the broader adoption of therapeutic proteins is the need to increase the stability of recombinant proteins to improve on their formulation and shelf lives, while maintaining their activities or efficacies.[5]

Efforts to increase or enhance the stability of biological molecules are limited by the molecular tools provided by nature. Many approaches to stabilize proteins have been developed,[6,7] including directed evolution with the canonical amino acids,[8] applying principles learned from proteins of extremophiles,[6] or attaching proteins to a matrix material, such as surfaces or polymers.[9] While these approaches have all seen some success, it is rare that adding an electrostatic interaction would stabilize a protein by significantly more than 1 kcal/mol.[10−12] The advent of methods for incorporating non-canonical building blocks into proteins[13] has helped to overcome some limitations but continues to be constrained by the standard menu of noncovalent interactions that dictate molecular folding. We show for the first time that a more thermally stable protein [in this case, the model T4 lysozyme, or T4L (Figure 1A)] with increased enzymatic activity at elevated temperatures can be engineered by adding a single halogen atom to a tyrosine (Y) residue. This increased stability and activity can be attributed to a previously uncharacterized form of the halogen bond (XB) interaction in which an intramolecular hydrogen bond (HB) from the tyrosyl OH enhances the XB potential of the halogen.

XBs are analogous to HBs[14] and, although the physicochemical foundation remains debated,[15−17] their electrostatic nature is readily modeled by the σ-hole theory[18] (Figure 2). In this model, one lobe of a halogen's p_z orbital becomes depopulated when its valence electron is subsumed by the molecular σ-orbital of a covalent bond. The result is an electropositive σ-hole, which serves as the XB donor. However, the electronegative annulus around the waist makes the

Received: May 29, 2018
Published: June 19, 2018

DOI: 10.1021/acs.biochem.8b00603
Biochemistry 2018, 57, 4135−4147

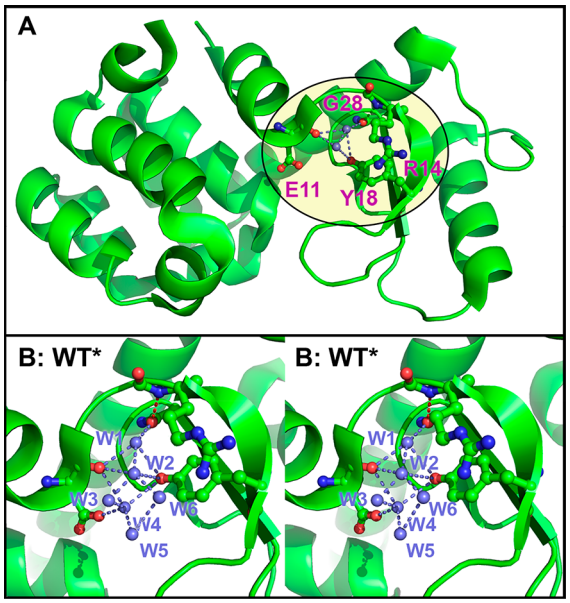

Figure 1. Crystal structure of pseudo-wild-type T4 lysozyme (WT*). (A) Overall structure of WT*, with the polypeptide backbone traced as a green ribbon. Atoms of the tyrosine 18 (Y18) residue, along with the interacting residues glutamate 11 (E11), arginine 14 (R14), and glycine 28 (G28), are shown as ball and stick models colored according to atom type (green for carbon, red for oxygen, and blue for nitrogen). Two water molecules that bridge the hydroxyl substituent of Y18 and the carbonyl oxygens of E11 and G28 are shown (interactions shown as dashes). The carbonyl oxygen of G28 forms a standard HB with the backbone amino nitrogen of R14 (shown as a dash, with an O···N distance of 3.1 Å). (B) Details (as a wall-eye stereoview) of the interacting water molecules that bridge from Y18 to E11, G28, and R14 (labeled W1–W6).

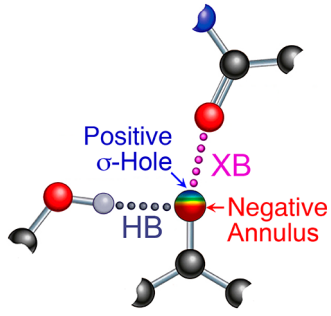

Figure 2. Amphoteric property of halogen substituents. The anisotropic charge distribution, as predicted by the σ-hole model,[18] allows the halogen to accept an HB from a hydroxyl and donate an XB to a carbonyl oxygen.

halogen amphoteric,[19,20] able to serve simultaneously as an HB acceptor perpendicular to the σ-hole.[21,22]

In biology, XBs define the binding specificity and affinity of halogenated enzyme inhibitors[23] and have been shown to affect the folding of nucleic acids,[24−26] making them important tools for both medicinal chemistry[27−30] and biomolecular engineering.[20,31] To study the effects of XBs on protein folding, we had previously replaced the OH of a tyrosine (Y18) with an XB-forming halogen[32] and showed that the interaction will partially rescue the stability of T4L, relative to a site that cannot form an XB, but not back to that of the parent (WT*) enzyme. The Y18 hydroxyl is neighboring but not sufficiently close to form HBs with carbonyl oxygens of glutamate 11 (E11) and glycine 28 (G28). Instead, these groups are bridged by water molecules from Y18 to E11 and to G28 (W2 and W1, respectively, in Figure 1B), which were found to be critical to both the stability and the function of T4L.[32] When the OH of Y18 is removed (as in a Y18F construct), W1 shifts in position to effectively fill the void to partially rescue the stability of the protein. Replacing the OH of Y18 with a methyl group (as in a $Y18^{Me}F$ construct) results in the loss of W2 and a large associated decrease in protein stability. There are now >300 studies of T4L point mutations that demonstrate the power of this system to study structure−energy−function relationships in a well-controlled protein,[33] and it is the rare instance that an engineered mutation, including those with halogenated amino acids,[32] results in significant stabilization (≥1° increase in the melting temperature, T_M) of the enzyme.

In this study, a series of T4L constructs were designed in which Y18 is halogenated at the *meta* position (^{mX}Y18-T4L, where X = Cl, Br, or I), leaving the critical OH substituent intact. The halogens are placed to potentially form an XB to the carbonyl oxygen of G28 located in a tight loop region near the enzyme active site and thus enhance T4L stability. The G28 oxygen forms a standard (3.1 Å) HB to the backbone amino nitrogen of arginine 14 [R14 (Figure 1A)]. However, a small void space was identified within this loop region that could potentially accommodate a halogen to form an XB to this G28 oxygen in a geometry that is perpendicular to the O···H−N HB. The theory that XBs are orthogonal interactions to this type of HB[34] would suggest that the halogen interaction should not disrupt the protein interaction. We had previously shown that the energy of an O···H−N HB is not perturbed with the addition of an XB, and vice versa. Our prediction, therefore, was that a ^{mX}Y18-T4L could potentially form an XB to G28, which would augment the existing HBs and, thus, increase the stability of the overall protein.

Ohtake et al.[35] had previously shown that incorporating seven ^{mX}Y residues (X = Cl or Br) increased glutathione *S*-transferase stability by ∼5.5 kcal/mol, not through XBs, but by filling void spaces in the protein core and enhancing the HBs already present through standard inductive effects. Unnatural amino acids as ligands have previously been shown to form stabilizing XBs to protein backbones,[36] as many other halogenated ligands do.[27,37−39] We demonstrate here that introducing a single ^{mX}Y into a protein structure can by itself increase the thermal stability of T4L by 3 kcal/mol and that this increased stability can be attributed to an HB-enhanced XB (abbreviated here as an HeX-B to simplify discussion). This distinctive interaction was revealed from quantum mechanical (QM) analyses of the crystal structures of ^{mX}Y18-T4Ls and their relationships to protein stability and enzymatic activities.

MATERIALS AND METHODS

Site-Directed Mutagenesis and Protein Expression. All T4 lysozyme (T4L) constructs started with the gene of pseudo-wild-type (WT*) protein, the T4L double mutant C54T/C97A,[40] with the DNA sequence encoding a six-His tag appended at the C-terminus to facilitate protein purification. The ^{mX}Y18-T4L constructs (^{mCl}Y18, ^{mBr}Y18, and ^{mI}Y18) had the codon for Y18 replaced with an AMBER (TAG) codon.[41] The modified DNA sequences were inserted into the pBAD vector for DNA amplification in DH5α *Escherichia coli*.[32]

The expression vector for the WT* construct was transformed into BL21 (DE3) pLysS *E. coli*. Transformed cells were

DOI: 10.1021/acs.biochem.8b00603
Biochemistry 2018, 57, 4135−4147

grown in 2× YT medium with the appropriate antibiotics (ampicillin and chloramphenicol) and incubated at 37 °C while being shaken at 250 rpm until an OD_{600} of 0.4−0.6 was reached. The cells were induced with the addition of arabinose directly to the cultures to a final concentration of 0.2% (w/v) and allowed to grow for an additional 3 h. Subsequently, the cells were harvested by centrifugation at 2200 relative centrifugal force (RCF). Thereafter, the supernatant was decanted, and the bacterial pellet was stored at −80 °C.

Expression vectors for the ^{mX}Y18-T4L constructs were co-transformed into BL21ai *E. coli* with the *pDule2-Mb-ClTyrRS-C6* plasmid that contains the orthogonal *Mb* $tRNA_{CUA}$ and 3-halo-Tyr amino acyl-tRNA synthetase. After being rescued, the transformed cells were stored at −80 °C. Starter cultures of NIM medium[42,43] containing appropriate antibiotics (ampicillin and spectinomycin) were inoculated with these cell stocks and allowed to grow at 37 °C for 12 h while being shaken at 250 rpm. Then, 5 mL of the starter cultures was used to, in a 2 L culture flask, inoculate 500 mL of AIM[42,43] medium containing the appropriate antibiotics (ampicillin and spectinomycin), but lacking arabinose. After inoculation, the cultures grew at 37 °C while being shaken at 250 rpm. When an OD_{600} of ∼1.0 was reached, the noncanonical amino acid (3-chloro-L-tyrosine, 3-bromo-L-tyrosine, or 3-iodo-L-tyrosine) was added to the cultures to obtain a final concentration of 1.0 mM. The 3-halo-L-tyrosines were supplied from Ark Pharm, Inc. The cultures continued to grow at 37 °C while being shaken at 250 rpm. When an OD_{600} of 3.0−4.0 was reached, the cultures were induced with a final concentration of 0.2% (w/v) arabinose. After induction, the bacterial growth was continued for 3 h at 37 °C while the sample was being shaken at a reduced speed of 100 rpm. Finally, after expression for 3 h, the cells were harvested by centrifugation at 4000 RCF, the supernatants were decanted, and the bacterial pellets were stored at −80 °C.

Protein Purification. The frozen bacterial pellets were suspended in 35−45 mL of a 9:1 buffer A/buffer B mixture [buffer A consisting of 40 mM potassium phosphate (pH 7.4), 500 mM sodium chloride, and 0.02% (w/v) sodium azide and buffer B consisting of 40 mM potassium phosphate (pH 7.4), 500 mM sodium chloride, 500 mM imidazole, and 0.02% (w/v) sodium azide] and thawed in a 37 °C water bath for 15 min. Subsequently, the cells were lysed by sonication on ice for 3 × 30 s using a Branson Sonifier 450 sonicator (duty cycle of 70%, output control of 7). After cell lysis, the homogeneous suspension was centrifuged in a Beckman model J2-21 centrifuge equipped with a JA-20 rotor at 16000 rpm and 4 °C for 30 min. The supernatant was decanted and filtered twice, first through a 0.45 μm pore syringe filter and thereafter through a 0.22 μm pore filter. The filtered cell lysate was loaded, applying 10% buffer B, onto a 5 mL HisTrap HP column on an ÄKTA start FPLC system. Nonbound protein was washed out with 15% buffer B over 5 column volumes. The His-tagged T4L construct was eluted with a gradient of 20 to 100% buffer B over 13 column volumes. Selected fractions were combined and concentrated to 1 mL in an Amicon Ultra-15 10K (Millipore) centrifugal device [10000 molecular weight cutoff (MWCO)] in an Eppendorf 5810 R centrifuge at 4000 rpm and 4 °C. The concentrated protein solution was then loaded onto a gravity-fed Sephadex G-50 fine column equilibrated in buffer specific for either crystallization or differential scanning calorimetry (DSC) [crystallization buffer consisting of 100 mM sodium phosphate (pH 7.0), 500 sodium chloride, and 0.02% (w/v) sodium azide and DSC buffer consisting of 20 mM glycine-HCl (pH 3.5), 80 mM sodium chloride, and 1 mM EDTA]. After gel filtration, the selected fractions were combined and used for crystallization or DSC experiments.

Protein Crystallization. After gel filtration purification using the crystallization buffer, described above, the combined and selected fractions were concentrated to 13−20 mg/mL using an Amicon Ultra-15 10K (Millipore) centrifugal device (10000 MWCO) in an Eppendorf 5810 R centrifuge at 4000 rpm and 4 °C. Crystals of the ^{mX}Y18-T4L constructs were grown at 18 °C using the hanging drop vapor diffusion method with a 2:3 to 7:3 ratio of protein to precipitant solution [precipitant solutions consisting of 2.0−2.4 M potassium phosphate (pH 6.5−7.4), 50 mM 2-hydroxyethyldisulfide, and 50 mM 2-mercaptoethanol] with a final protein concentration of 8−10 mg/mL in a 3.5−4.0 μL total drop volume, similar to the process previously described.[32] Diffraction quality crystals grew after 2−5 days for the ^{mBr}Y18 and ^{mCl}Y18-T4L constructs and after ∼2 weeks for the ^{mI}Y18-T4L construct. The crystals were harvested using a cryo-loop, flash-frozen, and stored in liquid nitrogen until X-ray data were collected.

X-ray Data Collection and Structure Determination. X-ray diffraction data were collected on crystals held under a cryogenic nitrogen stream (100 K) on the Advanced Light Source (ALS) Beamline 4.2.2 at Berkeley National Laboratory (1.00 Å, Research Detectors Inc. complementary metal-oxide-semiconductor 8 M detector). Diffraction data from the ALS beamline were reduced using XDS[44] and the CCP4 suite.[45] X-ray data were phased by molecular replacement, applying the atomic coordinates of WT* [Protein Data Bank (PDB) entry 1L63[12]] as the starting model, yielding initial models with R_{work} values that ranged from 29.6 to 39.5% and R_{free} values that ranged from 30.9 to 41.2%. Subsequent refinement of the structure using the PHENIX suite of crystallographic software[46] resulted in final structures with R_{work} values that ranged from 17.7 to 19.9% and R_{free} values that ranged from 20.8 to 23.2% (Table S1).

Differential Scanning Calorimetry (DSC). After gel filtration purification [DSC buffer (pH 3.5)], as described above, the combined fractions of the pure T4L construct were diluted to a concentration of 0.3 mg/mL with DSC buffer. Aliquots of 900 μL were prepared and stored at −80 °C. A low pH was used to help promote reversible folding.[47] Melting curves were collected on a TA Instruments Nano DSC model 602001 instrument under constant pressure (3.0 atm) with all samples matched against identical buffer in the reference cell. Samples were equilibrated for 600 s, followed by melting data collection through heating cycles from 10 to 90 °C at a scan rate of 0.75 °C/min. The reversibility was confirmed for all constructs by performing a cooling scan from 90 to 10 °C at a scan rate of 0.5 °C/min and a subsequent heating cycle. A minimum of 10 replicate experiments were conducted for each T4L construct. Melting data were analyzed, and thermodynamic parameters, including the specific heat capacities (ΔC_p), were determined using NanoAnalyze Data Analysis, version 3.6.0, from TA Instruments. The melting temperatures (T_M) and enthalpies (ΔH_M) were extracted using the TwoStateScaled model for fitting the experimental data. The $\Delta H_{fit}/\Delta H_{cal}$ ratios were all in the range of 0.97−1.01; the Aw values were in the range of 0.99−1.05, and the standard deviation of the fits was <1.6 for all experiments.

DOI: 10.1021/acs.biochem.8b00603
Biochemistry 2018, 57, 4135−4147

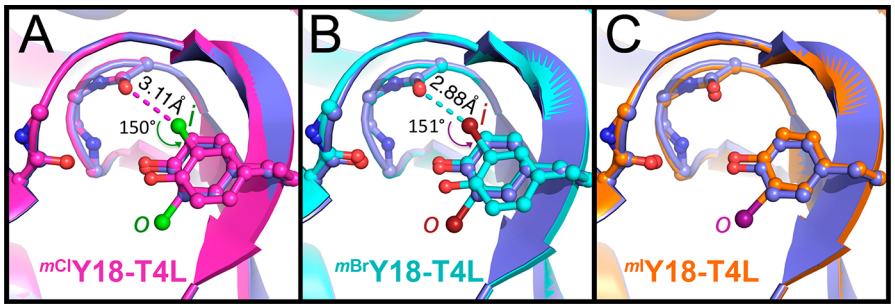

Figure 3. Crystal structures of $^{m\mathrm{X}}$Y18-T4L constructs. (A) Overall structure of the chlorinated $^{m\mathrm{Cl}}$Y18-T4L (magenta backbone trace and carbon atoms) overlaid on WT*-T4L (blue trace and carbon atoms). The $^{m\mathrm{Cl}}$Y18 side chain sits with Cl (green) either inside the loop toward the G28 oxygen (*i*-rotamer) or outside this loop (*o*-rotamer). The *o*-rotamer overlays nearly exactly with WT*, while the Y18 side chain of the *i*-rotamer is slightly shifted away from G28. The 3.11 Å Cl···O distance from $^{m\mathrm{Cl}}$Y18 to G28 is 95% of the sum of the van der Waals radii ($\sum R_{\mathrm{vdW}}$), while the angle of approach (O···Cl−C) is a shallow 150°. (B) Overall structure of brominated $^{m\mathrm{Br}}$Y18-T4L (cyan) overlaid on WT*-T4L (blue). As with the chlorinated construct, Br (brown) is in either the *i*- or *o*-rotamer. The *o*-rotamer, again, overlays nearly exactly with WT*, while the Y18 side chain of the *i*-rotamer is more shifted significantly away from G28. The 2.88 Å Br···O distance in $^{m\mathrm{Br}}$Y18 is 85% of the $\sum R_{\mathrm{vdW}}$, and the angle of approach (O···Br−C) is also shallow at 151°. (C) Overall structure of iodinated $^{m\mathrm{I}}$Y18-T4L (orange) overlaid on WT*-T4L (blue). Unlike the Cl and Br constructs, this construct places the iodine (purple atom) only in the *o*-rotamer position and, therefore, does not make a short interaction with G28.

Quantum Mechanical (QM) Calculations. QM energies and electrostatic potential maps (ESPs) were calculated using Gaussian 09 revision E.01[48] with the Møller−Plesset second order (MP2) in a cyclohexane solvent (D = 2 relative to a vacuum). This low-dielectric solvent model is appropriate for calculations on systems that involve explicit solvent and short distances between interacting atoms, as is the case in this study, and reflects the low dielectric expected for a protein interior.[49] Basis set superposition errors (BSSEs)[50] were determined from a separate counterpoise gas phase calculation and directly summed into the calculated solvent phase energy. Polarizable basis sets, including dispersion, were applied (aug-cc-PVTZ[51] for $^{m\mathrm{Cl}}$Y18 and $^{m\mathrm{Br}}$Y18 and extended to $^{m\mathrm{I}}$Y18 with aug-cc-PVTZ-PP from EMSL basis set exchange). The strategy for QM calculations applied here had previously been validated against experimental XB geometries and energies in model DNA junction systems.[52−54] The atomic coordinates of the interacting residues (Y18 and G28) were taken from the refined structures of each construct. Residue 18 was reduced to 2-halophenol, and residue 28 was reduced to *N*-methylacetamide (NMA) to decrease computational time. Hydrogen atom positions were geometry-optimized with a semiempirical AM1 calculation. The torsional angle, δ, of the hydroxyl hydrogen is manually rotated to determine its contribution to the HeX-B.

Turbidity Assay. The activities of the T4L constructs were monitored through a standard cell clearing assay.[55,56] *Micrococcus lysodeikitcus* bacteria were grown in 50 mL of 2× YT medium overnight at 37 °C while being shaken at 250 rpm. Then, the culture was centrifuged in an Eppendorf 5810 R centrifuge at 4000 rpm at 4 °C for 15 min. The supernatant was decanted, and the cell pellet diluted in a 1:1 mixture of 50 mM monobasic and 50 mM dibasic sodium phosphate solutions until an OD_{450} of 1.0 was reached. Bacterial samples of 1.0 mL were prepared and stored at −80 °C. After the samples had thawed, the purified and concentrated T4L construct in crystallization buffer was added to the bacterial sample to reach a final concentration of 0.1 mg/mL. The absorbance change over time was measured at room temperature (23 °C) and 40 °C. Three or four replicates of each construct were run for each temperature.

RESULTS

Structures of $^{m\mathrm{X}}$Y18-T4L Constructs. The crystal structures of the $^{m\mathrm{X}}$Y18-T4Ls ($^{m\mathrm{Cl}}$Y18, $^{m\mathrm{Br}}$Y18, and $^{m\mathrm{I}}$Y18), determined from 1.35 Å to 1.65 Å resolution (Table S1 and Figure S1), are all isomorphous with the parent WT* (Figure 3), allowing any observed structural perturbations to be analyzed relative to each other, and relative to their effects on the constructs' stabilities and activities. The $^{m\mathrm{X}}$Y18 side chain of each construct sits in a pocket formed by a pair of antiparallel loops and is rotated to place the halogen inside this pocket (*i*-rotamer) pointed toward G28 or outside the pocket (*o*-rotamer) exposed to the solvent (Figure 3). The *i*-rotamer propensity increases as the halogen becomes smaller (Table 1).

Table 1. Crystallographic Analysis of Ratios of *i*-Rotamer to *o*-Rotamer, XB Geometries (where observed), and Solvent Accessible Surfaces (SASs) in the $^{m\mathrm{X}}$Y18-T4L Constructs (X = Cl, Br, or I)

construct	*i*-rotamer:*o*-rotamer	$R_{\mathrm{X\cdots O}}$ ($\%\sum R_{\mathrm{vdW}}$)[a]	θ_1[b]	SAS (% max)[c]
$^{m\mathrm{Cl}}$Y18-T4L	54:46	3.11 Å (95%)	150°	17.3 Å^2 (13.8%)
$^{m\mathrm{Br}}$Y18-T4L	22:78	2.88 Å (85%)	151°	28.9 Å^2 (21.8%)
$^{m\mathrm{I}}$Y18-T4L	0:100	not applicable	not applicable	17.1 Å^2 (11.9%)

[a]$\%\sum R_{\mathrm{vdW}}$ is the percent of the sum of the standard van der Waals radii of the halogen to oxygen (X···O) interacting pair. [b]θ_1 is the angle of approach of the oxygen acceptor to the halogen, ∠(C−X···O). [c]Solvent accessible surfaces for halogen atoms were calculated using PyMol.[87] The percent relative to maximum exposure (% max) was calculated relative to the exposure of each halogen in an isolated $^{m\mathrm{X}}$Y amino acid residue (SAS for Cl of $^{m\mathrm{Cl}}$Y = 124.8 Å^2, SAS for Br of $^{m\mathrm{Br}}$Y = 132.7 Å^2, and SAS for I of $^{m\mathrm{I}}$Y = 143.6 Å^2).

The structure of the loop is invariant among all constructs, with the O···H−N HB distance (from G28 to R14) varying by <0.1 Å relative to WT* (Tables S2−S5). This loop region in the crystal structure is, therefore, very rigid, sterically constraining the size of the halogen that is accommodated and consequently its potential to participate in an XB.

The halogens of the *i*-rotamers of $^{m\mathrm{Cl}}$Y18-T4L and $^{m\mathrm{Br}}$Y18-T4L are seen to form short-range interactions with the

DOI: 10.1021/acs.biochem.8b00603
Biochemistry 2018, 57, 4135−4147

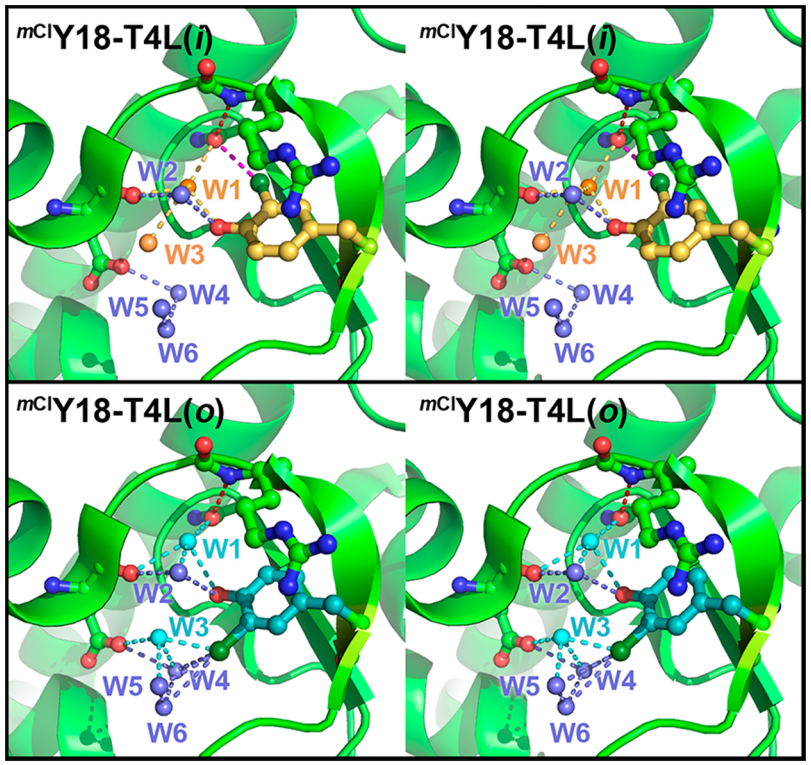

Figure 4. Stereoimage of the chlorinated ^{mCl}Y18-T4L construct with its waters of interaction. The top panels show the rotamer with the chlorine (emerald green) sitting inside [^{mCl}Y18-T4L(*i*), carbon atoms colored yellow] the loop. Waters are labeled W1−W6, with those that are in positions nearly identical to those of WT* colored and labeled in blue and those in positions unique to the *i*-rotamer colored and labeled in yellow (along with the carbons of the Y18 side chain). The bottom panels show the rotamer with the bromine sitting outside [^{mCl}Y18-T4L(*o*), carbons colored cyan] the loop. Waters are labeled W1−W6, with those that are in positions nearly identical to those of WT* colored and labeled in blue and those in positions unique to the *o*-rotamer colored and labeled in cyan.

carbonyl oxygen of G28 (Figure 3A,B). The Cl···O distance in ^{mCl}Y18-T4L is ∼95% of the sum of the standard van der Waals radii ($\sum R_{vdW}$) of the interacting atoms, near the optimum distance for biological XBs,[20] while the Br···O distance in ^{mBr}Y18-T4L is much shorter at ∼85%. The angles of approach of the oxygen acceptor to the halogen (θ_1 = 150° for O···Cl−C, and θ_1 = 151° for O···Br−C) are shallow relative to the ideal linear approach (θ_1 = 180°); however, these geometries are well within the range of XB interactions observed in biological systems[20] and, as will be discussed later, are accommodated by additional polarization of the halogens in this particular system. In addition, the approach angles of halogen to the acceptor HB (X···O···N) are 80.6° for X = Cl and 82.2° for X = Br, which are consistent with the XBs being an orthogonal interaction (geometrically perpendicular and energetically independent) to the HB.[34] Thus, we are confident in classifying these interactions as XBs.

The small displacement of the ^{mCl}Y18-T4L aromatic side chain in the *i*-rotamer from the *o*-rotamer position is likely an attempt to pull the halogen into a more linear XB geometry. The larger displacement of the ^{mBr}Y18-T4L side chain away from G28, however, suggests destabilizing steric effects in the *i*-rotamer even as the halogen forms a short XB interaction. This balance between an XB attractive and steric repulsive force (and potentially bonding forces from distortion of the side chain) would account for the lower *i*-rotamer:*o*-rotamer ratio of the bromo construct. The fact that the larger iodine of ^{mI}Y18-T4L is entirely in the *o*-rotamer supports this interpretation. Given that none of the constructs are entirely in the *i*-rotamer position, the question is whether the XB interactions are actually stabilizing. We will address this question later by comparing the melting temperature (T_M) and enthalpy (ΔH_M) in solution of each ^{mX}Y18-T4L construct to those of the parent WT* enzyme.

Solvent Structure. The constellation of waters around E11, Y18, and G28 seen in the WT* structure (Figure 1B) remains mostly intact in the halogenated constructs, except to accommodate the halogens in their *i*- or *o*-rotamers (Figure 4, Figures S2 and S3, and Tables S2−S5). For ^{mCl}Y18-T4L, the waters that bridge Y18 to E11 (W2−W6) are seen in positions similar to those in WT*, with the exceptions of W1 and W3. In the chlorinated construct, the position of W1, which is particularly important in stabilizing the T4L protein,[32] is filled by two partially occupied water molecules, each very close (within 1.8 Å) to the other. In addition, one of these waters sits unusually close to the OH of the Y18 side chain of the *o*-rotamer. We therefore interpreted this water as being a single molecule occupying two mutually exclusive positions: one assigned to the *o*-rotamer (W1-*o*, sitting in nearly the same position as W1 in WT*) and the other to the *i*-rotamer (W1-*i*, repositioned to sit in the aromatic plane) of the ^{mCl}Y18 residue. Although not as important as W1 in terms of defining protein stability, W3 also shows two partially occupied positions, one that forms an HB to the Cl of the *o*-rotamer (assigned as W3-*o*) and one that does not (assigned as W3-*i*).

The waters around ^{mBr}Y18-T4L (Figure S2 and Table S4) show patterns similar to those in the ^{mCl}Y18-T4L structure, with certain solvent positions (including W1) occupied by molecules that are associated with the *i*-rotamer or the *o*-

DOI: 10.1021/acs.biochem.8b00603
Biochemistry 2018, 57, 4135−4147

Table 2. DSC-Measured Melting Temperatures (T_M), Enthalpies (ΔH_M), and Heat Capacities of the WT* and ^{mX}Y18-T4L Constructs (X = Cl, Br, or I)

construct	T_M (°C)	ΔH_M (kcal/mol)	ΔS_M (cal mol^{-1} K^{-1})[a]	ΔC_p (kcal mol^{-1} K^{-1})
WT*	57.30 ± 0.01	120.2 ± 0.5	363.8 ± 1.5	2.6 ± 0.2
^{mCl}Y18-T4L	58.28 ± 0.01	122.9 ± 0.4	370.7 ± 1.2	2.9 ± 0.3
^{mBr}Y18-T4L	57.36 ± 0.02	119.2 ± 0.4	360.6 ± 1.1	3.3 ± 0.2
^{mI}Y18-T4L	56.78 ± 0.01	115.5 ± 0.6	350.1 ± 1.9	2.8 ± 0.1

[a] ΔS_M is the melting entropy calculated as $\Delta H_M/T_M$.[88]

rotamer. The solvents in ^{mI}Y18-T4L (Figure S3 and Table S5) are similar to WT*, except that W1 is entirely missing, a consequence of the Y18 side chain being pushed closer to the carbonyl oxygen of G28, which has either completely displaced this solvent molecule or made it less specific in its positions (thereby making it unobservable in the electron density map).

Thermal Stabilities of ^{mX}Y18-T4L Constructs. Differential scanning calorimetry (DSC) was used to determine how the conformational features seen in each of the crystal structures affect the stability of the protein. This protein system allows precise determination of melting temperatures and enthalpies and, thus, allows us to accurately assign thermodynamic values to molecular interactions associated with specific structural modifications.[57]

The DSC-measured T_M of ^{mI}Y18-T4L (Table 2), with the iodine entirely in the exposed *o*-rotamer position, is ∼0.5 °C lower than that of WT*, which is consistent with our previous observation[32] that a protein is destabilized when a hydrophobic methyl or halogen substituent[58] is added to a solvent-exposed position and with previous studies on the effects of hydrophobic side chains on T4L stability.[59] This hydrophobic effect is reflected in the increased ΔC_p value. The ^{mBr}Y18-T4L construct has T_M and ΔH_M values that are very similar to that of WT*, indicating that the stabilizing XB in the *i*-rotamer nearly exactly counterbalances the destabilizing effects of steric repulsion of this buried placement and the exposure in the *o*-rotamer. The most interesting case is that of the ^{mCl}Y18-T4L construct, which shows an ∼1 °C increase in T_M and a 2.7 kcal/mol increase in ΔH_M versus those of WT*. Together, the results show that the increased stability of the protein, as measured by the T_M and ΔH_M, is dependent on the ability of the halogen to form an XB interaction in the *i*-rotamer (Figure 5). Thus, for the first time, a more thermally stable protein was engineered by introducing a halogenated, in this case chlorinated, unnatural amino acid.

The entropy of melting (ΔS_M) can be calculated from the experimental ΔH_M and T_M values for each construct (Table 2). The resulting ΔS_M for ^{mCl}Y18-T4L is ∼7 cal mol^{-1} K^{-1} higher than that of WT*, suggesting that the XB makes the protein more conformationally rigid. The alternative interpretation would be that ΔS_M is defined by changes in the solvent structure, particularly because the halogens of the ^{mX}Y residues are hydrophobic.[58] The expectation is that if the halogen is already exposed to solvent, as is the case for the *o*-rotamer of ^{mI}Y18-T4L and ^{mBr}Y18-T4L constructs, the entropic change upon melting would be smaller than if the halogen were more buried, as in the *i*-rotamer of ^{mCl}Y18-T4L. To determine whether solvent effects are the primary determinant of ΔS_M, we calculated the solvent accessible surfaces [SASs (Table 1)] of the halogens in the *i*-rotamer (when present) and *o*-rotamer conformations. The halogens in the *i*-rotamer of ^{mCl}Y18-T4L and ^{mBr}Y18-T4L are fully buried, as reflected in SASs of 0 Å^2. The *o*-rotamers of all the halogenated constructs showed some

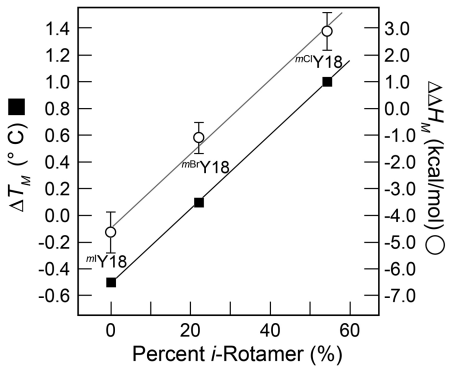

Figure 5. Differences in melting temperatures [ΔT_M (■)] and in melting enthalpies [$\Delta\Delta H_M$ (○)] for ^{mX}Y18-T4L (X = Cl, Br, or I) vs WT* constructs of T4 lysozyme. Standard deviations of the measured values are shown as error bars.

degree of exposure to solvent, with the Br of ^{mBr}Y18-T4L being most exposed and the I of ^{mI}Y18-T4L being the least, particularly in terms of the percentage relative to the exposure of an isolated halogenated tyrosine. Unlike our earlier study,[32] the effect of each halogen in an exposed versus buried site is internally controlled here. This observation is contrary to what was expected, but careful analyses of the structures show that the side chain of Arg14 is pulled within HB distance (3.1 Å) of the I, thus burying a significant portion of the halogen surface that is otherwise solvent-exposed in the other constructs. A comparison of the SAS and associated solvent free energies shows that they are not correlated to the ΔS_M values. The ΔS_Ms, however, are well correlated with the occupancies of the *i*-rotamers (R = 99.3%), indicating that the interactions of the halogens with the loop are the primary determinants of the entropic effects on the protein structure. The DSC melting energies converted to $\Delta G°$ of stability at 40 °C follow exactly the trend for the T_Ms, showing that the XB renders ^{mCl}Y18-T4L overall more stable than WT* at high temperatures.

Extrapolation of the thermodynamic DSC thermodynamic parameters to the standard temperature (25 °C) indicates that the overall stabilities, as reflected in $\Delta G°$, for all of the halogenated constructs are lower than that of WT* at this lower temperature (Table 3). The resulting standard energies follow the general trend for the melting parameters previously reported for T4L,[33,60] except for those of ^{mBr}Y18-T4L ($\Delta H°$ and $\Delta S°$), which are calculated as being significantly lower than those of the other constructs. This singular outlier can be ascribed to the anomalously high ΔC_p of ^{mBr}Y18-T4L, which affects extrapolation of its DSC energies to room temperature (RT). This higher DSC-measured ΔC_p is indicative of a more hydrophobic system; ΔC_p values have been shown to be well correlated with SASs.[33,61−65] The experimental ΔC_p values listed in Table 2 are indeed well correlated with the SAS values in Table 1, as the percent of the maximum exposure of the

DOI: 10.1021/acs.biochem.8b00603
Biochemistry 2018, 57, 4135−4147

Table 3. Standard Enthalpies ($\Delta H°$), Entropies ($\Delta S°$), and Gibbs Free Energies ($\Delta G°$) of Stabilization Extrapolated to 25 and 40 °C from DSC Melting Energies (Table 2) of the WT* and ^{mX}Y18-T4L Constructs (X = Cl, Br, or I)

	25 °C			40 °C		
construct	$\Delta H°$ (kcal/mol)	$\Delta S°$ (cal mol^{-1} K^{-1})	$\Delta G°$ (kcal/mol)	$\Delta H°$ (kcal/mol)	$\Delta S°$ (cal mol^{-1} K^{-1})	$\Delta G°$ (kcal/mol)
WT*	−34.8	−91.7	−7.43	−74.5	−222	−5.07
^{mCl}Y18-T4L	−27.6	−67.6	−7.38	−70.5	−208	−5.31
^{mBr}Y18-T4L	−12.5	−20.8	−6.27	−61.9	−183	−4.73
^{mI}Y18-T4L	−26.9	−67.8	−6.71	−68.7	−205	−4.66

hydrophobic surface at Y18 (Figure S4), indicating that they reflect features of the crystal structures. Our interpretation is that the high ΔC_p of ^{mBr}Y18-T4L may not be applicable to a RT calculation, because of temperature effects on the *i*-rotamer:*o*-rotamer ratio of the ^{mBr}Y18 side chain. Our hypothesis is that near the T_M, relaxation of the protein permits the Br-substituted Tyr side chain to be better accommodated in the pocket and to form an XB, pushing a larger proportion to convert from the *o*- to *i*-rotamer. This allows more exposure of nonpolar surfaces upon melting, resulting in the observed ΔC_p[65,66] near the T_M for ^{mBr}Y18-T4L being higher than we would expect at RT. Indeed, extrapolation of the ^{mBr}Y18-T4L DSC data to RT using any of the other ΔC_p values in Table 2 results in energies that are comparable to those of the other T4L constructs in this study. Similar effects on ΔC_p would not be expected for either the Cl or I construct, because the side chain of ^{mI}Y18-T4L is not seen to form an XB, while the Cl of ^{mCl}Y18-T4L forms a stable XB. The XB favoring the buried *i*-rotamer of ^{mBr}Y18-T4L, however, is constricted by the steric repulsion that favors the exposed *o*-rotamer. In this way, the brominated construct exposes more hydrophobic surface upon thermal unfolding, which led to the anomalously high DSC-measured ΔC_p value and the unexpectedly low $\Delta H°$ and $\Delta S°$ values from extrapolation to RT.

Enzymatic Activities of ^{mX}Y18-T4L Constructs. The thermal stabilities of T4L and its various mutants are correlated with the level of enzymatic activity.[57] Thus, we applied the standard bacterial clearing assay to monitor the effects of halogenation on the activity and, in addition, provide additional support for their observed effects on the thermal stability of the enzyme. At RT (23 °C), the activities of the ^{mX}Y18-T4L constructs were all lower than that of WT* (Figure 6) and, with the exception of that of ^{mBr}Y18-T4L (Figure S5), are consistent with the $\Delta G°$ values calculated from the DSC melting energies (Table 3). At an elevated temperature (40 °C), the activity of the iodinated construct was not significantly changed but that of the brominated and chlorinated enzymes increased relative to that of WT*, with ^{mCl}Y18-T4L becoming 15% greater than the native enzyme. The temperature at which ^{mCl}Y18-T4L would become more stable than WT* is predicted from extrapolation of the DSC values to be ∼35 °C, which is also where we would expect the chlorinated enzyme to become more active. These general trends in activity at low and high temperatures follow and, therefore, confirm the DSC melting results (with the singular exception of ^{mBr}Y18-T4L extrapolated to 25 °C, as discussed above) and serve to bridge the melting properties measured at high temperatures and the structural features of crystals grown at low temperatures. Thus, we have shown for the first time that an XB can be specifically engineered not only to increase the thermal stability of a protein but also to increase its activity at elevated temperatures.

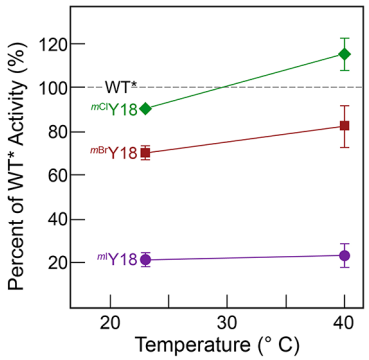

Figure 6. Enzymatic activities of ^{mX}Y18-T4L constructs, as a percent of WT* activity. The enzymatic activity of each halogenated construct (Cl in green diamonds, Br in red squares, and I in purple circles) is compared to that of WT* (defined as 100% and indicated by the dashed line) at 23 and 40 °C.

Structure−Stability/Activity Relationships: The Hydrogen-Bond-Enhanced Halogen Bond. The thermal stabilities of each construct, as reflected in the DSC-measured melting temperatures (T_M) and enthalpies (ΔH_M) (Table 2), are correlated with the percent *i*-rotamer (Figure 5). The interactions (attributed here to XBs) within the loop convey stability to the ^{mX}Y18-T4L constructs, while exposure of the halogen to a solvent (similar to that previously seen with halogenated and methylated T4L analogues[32]) destabilizes the protein. These DSC values, however, may underestimate the stabilizing potential of the XB, particularly in the ^{mCl}Y18-T4L construct, which places only 54% of the Cl in the *i*-rotamer position. If the Cl of ^{mCl}Y18-T4L were entirely in the XB position, the ΔH_M would be predicted to be 5.4 kcal/mol higher than that of WT*. In addition, the T_Ms are well correlated with their ΔH_Ms (a 1 kcal/mol increase in ΔH_M results in an ∼0.2° increase in T_M).

Even at ∼3 kcal/mol, the increase in ΔH_M measured for ^{mCl}Y18-T4L is significantly larger than that previously determined for Cl (0.5 kcal/mol) in a model DNA junction but comparable to those of Br and I (1.6−4.6 kcal/mol).[24,25,53] We attribute this remarkably stronger Cl effect to an XB that is enhanced by an intramolecular HB from the hydroxyl substituent to the negative annulus of the halogen. The electrostatic potential (ESP) surface (Figure 7) calculated for 2-halophenol (a model for the ^{mX}Y18 side chain) shows that the σ-holes of halogen substituents become enhanced as the OH rotates from an angle δ of 180° (*trans*-OH) to an angle δ of 0° (*cis*-OH, pointing toward and within H-bonding distance of the halogen). This enhancement is interpreted as resulting from polarization of the electron density by the HB toward the

DOI: 10.1021/acs.biochem.8b00603
Biochemistry 2018, 57, 4135−4147

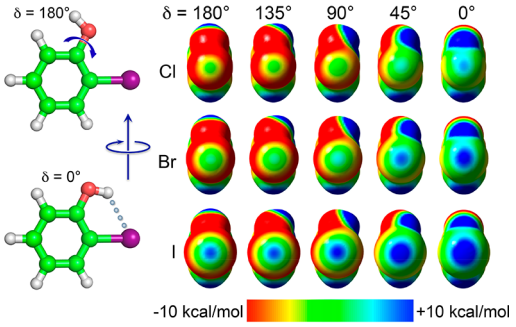

Figure 7. Effect of OH rotations on the electrostatic potential (ESP) of 2-halophenol. The QM-calculated ESPs are mapped onto the atomic surfaces of 2-halophenol, where the halogen is Cl, Br, or I. The map shows ESP from 10 to −10 kcal/mol of interaction energy to a positive point charge, reflecting a surface charge that ranges from positive (blue) to negative (red) on the halogen surface. The ESP is calculated as the OH is rotated from an angle δ of 180° (non-HB *trans*-OH orientation) to an angle δ of 0° (HB *cis*-OH orientation), in 45° increments. The neutral-charge angle (where the ESP ≈ 0) extends from an average of ∼163° (Cl, Br, and I) at an angle δ of 180° to ∼135° at an angle δ of 0° (compared to an average of 157° for halobenzenes).

$p_{x,y}$ orbitals and away from the σ-hole, which renders the ESP for Cl comparable to that of the Br in bromobenzene.[18,23]

The effect of the enhanced σ-hole on the XB donor ability of the Cl can be appreciated by comparing the QM-calculated XB energies (E_{MP2}) for complexes of *N*-methylacetamide (NMA) with either chlorobenzene or 2-chlorophenol (a model for the XB complex between G28 and ^{mCl}Y18), positioned according to the ^{mCl}Y18-T4L crystal structure (Figure 8). For chlorobenzene, the Cl···O XB energy is only slightly favorable (E_{MP2} = −0.3 kcal/mol), as expected for the inherently weak XB potential of Cl. The Cl is an even weaker XB donor ($E_{X\text{-}MP2}$ = 0.06 kcal/mol) in the 2-chlorophenol complex with a *trans*-OH, reflecting the electron-donating property of the OH substituent, as suggested by calculations on ^{mI}Y-substituted insulin.[67] The *cis*-OH, however, forms an HB with the Cl, resulting in an enhanced XB (E_{MP2} = −1.4 kcal/mol relative to the *trans*-OH). This E_{MP2} is nearly identical to that of an iodine XB (−1.8 kcal/mol) that was previously shown to rescue protein stability.[32] Thus, the HB intensifies the σ-hole and extends the allowed angles of approach by the acceptor to the halogen, both of which enhance the XB potential of Cl, resulting in the HeX-B interaction. As the OH rotates from the *trans*-direction to the HeX-B *cis*-direction (Figure 7), the angle at which the calculated ESP switches from being a positive σ-hole to a negative annulus (a neutral-charge angle) is increased by 22−28° for the halogen substituent (from ∼160° to < 135° for bromophenol, for example), allowing the relatively shallow 150° approach of the oxygen acceptor seen in the crystal structures to be stabilizing Cl and Br XB interactions. The HB to the halogen itself contributes significantly (−1.8 kcal/mol) to the interaction and, together with the HeX-B, accounts for the ∼3 kcal/mol enhancement of the DSC ΔH_M for ^{mCl}Y18-T4L versus that of WT*.

Why are these HeX-Bs not seen in all of the ^{mX}Y18-T4L constructs? For iodine, the answer is simply that this large halogen does not fit into the pocket of the rigid loop. The *i*-rotamer:*o*-rotamer ratio of the Br in ^{mBr}Y18-T4L reflects an ∼0.8 kcal/mol difference between a buried and exposed halogen. Although the Br···O geometry suggests a relatively strong XB, the large displacement of the side chain of the *i*-rotamer would indicate that this very short distance interaction is largely offset by an unfavorable steric clash. This balance between the opposing forces would account for the apparent discrepancy between the $\Delta G°$ and activity at RT (Figure S5).

The answer to why only ∼50% of ^{mCl}Y18-T4L forms the HeX-B interaction comes again from considering the OH group, which has no sense for whether an XB is present. The

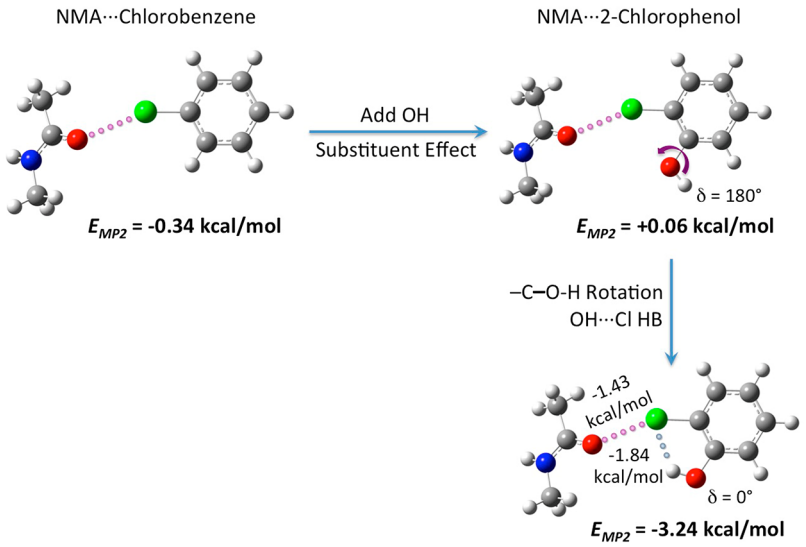

Figure 8. Quantum mechanics energies calculated at the MP2 level (E_{MP2}) for complexes of *N*-methylacetamide (NMA) with chlorobenzene (left) or 2-chlorophenol (right). Atomic positions of the components were defined by the coordinates of the crystal structure of the *m*-chlorotyrosyl side chain at position 18 and the peptide bond at G28 in the chlorinated T4 lysozyme construct (^{mCl}Y18-T4L). The intrinsic halogen bonding potential of a Cl substituent (reflected in the E_{MP2} of the NMA···chlorobenzene complex) is reduced by 0.4 kJ/mol with the introduction of the *o*-hydroxyl substituent, an electron-donating group, when this OH is rotated with the hydrogen away from the Cl (δ = 180°). Rotation of the OH so that it can form a HB to the Cl enhances the E_{MP2} of the NMA···2-chlorophenol complex (δ = 0°). This more favorable E_{MP2} can be parsed out to the energy of the HB itself but also to the enhanced energy of the XB.

DOI: 10.1021/acs.biochem.8b00603
Biochemistry 2018, 57, 4135−4147

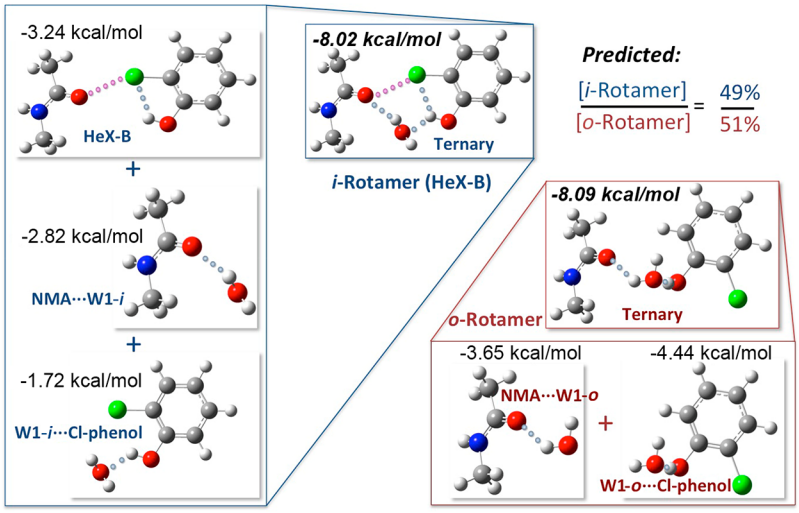

Figure 9. Quantum mechanics energies (E_{MP2}) calculated for the ternary complex of the *i*-rotamer (blue boxes) and *o*-rotamer (red boxes) forms of the ^{mCl}Y18-T4L construct. The energies calculated for the ternary complexes can be dissected out to the major contributing interactions: the HeX-B, NMA···W1, and W1···chlorophenol interactions for the *i*-rotamer (top left) and the NMA···W1 and W1···chlorophenol interactions for the *o*-rotamer (top right). Atomic coordinates for each model complex were taken from the crystal structure of the ^{mCl}Y18-T4L construct, with the water (W1) for each form assigned accordingly to the appropriate rotamer form (see Figure 4). Each W1 species was assigned to its appropriate rotamer based on their HB distances and potential clash with the Cl atom (W1-*o* would have clashed with the Cl in the *i*-rotamer form, but that assigned as W1-*i* did not show a Cl collision). Positions of hydrogens for the hydroxyl group of the chlorophenol model and the interstitial waters were optimized to yield the lowest-energy structures for each complex. The differences in their respective E_{MP2} values predict an [*i*-rotamer]:[*o*-rotamer] ratio of 49:51, which is nearly identical to the 54:46 ratio determined from the crystal structure.

Y18 hydroxyl is bridged by HBs to the carbonyl oxygen of E11 through a water [W1-*i* (Figures 3 and 9)],[32] which can form an HB to either the Cl (of the *i*-rotamer) or W1-*o* (the *o*-rotamer). The -OH···O═C distance between the Y18 hydroxyl and E11 carbonyl varies by <0.2 Å in ^{mCl}Y18-T4L (3.92 and 4.10 Å for the *i*- and *o*-rotamer, respectively, compared to 4.07 Å for WT*); consequently, the direct effects of the Cl on this interaction are expected to be minimal. If the OH of ^{mCl}Y18 is a donor to W1, it cannot simultaneously form an HB to the halogen and, thus, cannot enhance the XB capability; the approximate 1:1 *i*-rotamer:*o*-rotamer ratio suggests no preference for either Cl or W1. The higher energy of interaction of W1 with the ^{mCl}Y18 hydroxyl is a result of it being closer when this HB donor is not oriented toward the halogen. The QM energy calculated for a ternary complex of 2-chlorophenol, NMA, and W1 in their crystal structure conformations showed a <0.1 kcal/mol difference in E_{MP2} between the *i*- and *o*-rotamers, which would account for the near equal distribution among the rotamers (Figure 9). Furthermore, Abraham et al.[68] showed that 2-halophenols adopt a *trans*-OH in water but a *cis*-OH with a weak intramolecular HB between the hydroxyl and halogen in organic solvents. The pocket where ^{mX}Y18 sits is partially solvent exposed, resulting in the hydroxyl having only a slight preference as an HB donor to the Cl over W1.

DISCUSSION

In this study, we address the question of whether addition of an XB to augment a critical HB, by introducing an unnatural amino acid into the structure, would result in a more stable protein. The chlorinated ^{mCl}Y18-T4L construct demonstrates the potential application of XBs in increasing the stability and associated activity of an enzyme at elevated temperatures. We had previously shown that halogenation of proteins generally has the effect of destabilizing protein structure, if the halogen is exposed to solvent and, therefore, incapable of forming an XB.[32] This effect is recapitulated here, where the stabilities of the ^{mX}Y18-T4Ls are dependent on burying each halogen in a protein pocket (as reflected in the *o*- vs *i*-rotamers). The earlier study also showed that this destabilizing effect can be partially rescued if the halogen, particularly iodine with its very large σ-hole, can form an XB.[32] Again, we see this same effect with the current study; however, in this case, it is the chlorinated construct that forms the more stabilizing interaction, and the interaction is sufficiently strong not only to rescue the stability but also to increase it above that of WT*.

Although the ∼3 kcal/mol stabilization of T4L may seem to be small, it should be noted that proteins are stabilized by the concerted contributions of multiple low-energy, noncovalent interactions. Indeed, introducing a 3 kcal/mol interaction would convert metastable peptides and proteins to be fully stable structures, which would affect their functions.[69] Similarly, adding a 3 kcal/mol interaction to a ligand to its interaction with a protein target would reduce its dissociation constant by >2 orders of magnitude, which in turn could make such a ligand more attractive as a potential drug candidate.[30]

The stabilizing potential of an XB with a Cl donor had previously been determined to be very small (∼0.5 kcal/mol) in a DNA system.[25] A Cl-XB had also been estimated from calculations to contribute as much as 1.5 kcal/mol to stabilizing the β-hairpin conformation of a cyclic peptide,[70] one of the first demonstrations that an XB can potentially stabilize a protein-type conformation. Finally, it had been shown that addition of halogens that fill only void spaces contributes <0.8 kcal/mol per halogen atom.[35] Thus, the ∼3 kcal/mol stabilization seen here with the addition of a single chlorine atom is surprising, leading to the question of why the Cl-XB has such as strong effect even compared to the previous I-XB in this same T4L protein system.[32]

DOI: 10.1021/acs.biochem.8b00603
Biochemistry 2018, 57, 4135−4147

We attribute the improved ability of the Cl to serve as an XB donor to an HB-enhanced XB. The HeX-B represents a new and potentially powerful variation on the stand-alone XB, expanding the standard menu of noncovalent interactions that dictate molecular folding.[71−73] Because XBs and HBs share a common set of acceptors, their relationships can be complex.[74] The interaction described here, however, differs significantly from the orthogonal HB/XB interaction described previously in that the HB of the HeX-B is to the XB donor (as opposed to the acceptor) and enhances, rather than being energetically independent of, the stabilizing potential of the interaction. Upon addition of an HB donor (including OH, SH, or NH_2) next to a halogen, it is now possible to enhance its XB potential through a synergistic relationship, beyond tuning through standard inductive effects. This enhancement is expected to be even more dramatic (∼3−4 kcal/mol) for anionic oxygen XB acceptors compared to the neutral carbonyl acceptor in our study (Tables 4 and 5), extending the range of stabilization potentials to as much as 6.7 kcal/mol for an iodine HeX-B (compared to the 6 kcal/mol for very strong HBs in proteins[75]) when placed in an unconstrained biomolecular environment.

Table 4. Quantum Mechanical Energies (kilocalories per mole) for the Neutral Oxygen Halogen-Bond (XB) Acceptor of *N*-Methylacetamide Interacting with a Halobenzene or 2-Halophenol XB Donor[a]

XB Donor: Halobenzene			
Cl	Br		I
−0.75	−1.54		−2.61
XB Donor: 2-Halophenol			
δ	Cl	Br	I
0° (*cis*-OH)	−1.67	−2.36	−3.37
90°	−0.76	−1.55	−2.64
180° (*trans*-OH)	−0.52	−1.30	−2.43
$\Delta\delta$ (*cis* − *trans*)	−1.15	−1.06	−0.94

[a]The halogen to oxygen distances ($r_{X\cdots O}$) for the halobenzene and 2-halophenol XB donors were set to 92% of the sum of the respective van der Waals radii[89] of the halogen and the XB acceptor ($r_{Cl\cdots O}$ = 3.01 Å, $r_{Br\cdots O}$ = 3.10 Å, and $r_{I\cdots O}$ = 3.22 Å). The angle of approach of the acceptor oxygen to the X−C bond (θ_1 angle) was set at the optimum value of 180° for all calculations. For the 2-halophenol donor, the energies were calculated with the OH substituent rotated to align the hydrogen toward the halogen (δ = 0°), away from the halogen (δ = 180°), or perpendicular to the X···O bond (δ = 90°). The differences in energies between δ values of 0° and 180° are fairly independent of $r_{X\cdots O}$.

Table 5. Quantum Mechanical Energies (kilocalories per mole) for the Anionic Oxygen Halogen-Bond (XB) Acceptor of Hypophosphite Interacting with a Halobenzene or 2-Halophenol XB Donor[a]

XB Donor: Halobenzene		
Cl	Br	I
+0.03	−1.66	−4.29
XB Donor: 2-Halophenol		
δ	Cl	Br	I
0° (*cis*-OH)	−2.46	−4.16	−6.67
90°	0.00	−1.72	−4.35
180° (*trans*-OH)	1.05	−0.72	−3.45
$\Delta\delta$ (*cis* − *trans*)	−3.51	−3.44	−3.22

[a]The halogen to oxygen distances ($r_{X\cdots O}$) for the halobenzene and 2-halophenol donors were set to those seen in the crystal structures of the Cl2J ($r_{X\cdots O}$ = 2.88 Å), Br2J ($r_{X\cdots O}$ = 2.87 Å), and I2J ($r_{X\cdots O}$ = 3.01 Å) DNA constructs.[25] The angle of approach of the acceptor oxygen to the X−C bond (θ_1 angle) was set at the optimum value of 180° for all calculations. For the 2-halophenol donor, the energies were calculated with the OH substituent rotated to align the hydrogen toward the halogen (δ = 0°), away from the halogen (δ = 180°), or perpendicular to the X···O bond (δ = 90°).

More than 700 T4L variants have been characterized to date, very few of which result in more stable proteins, leading to the conclusion that it is very difficult to rationally engineer an enzyme with increased thermal stability and/or activity.[76] It has previously been shown that unnatural amino acids can be applied to engineer more stable proteins, primarily by introducing hydrophobic interactions[77] or unusual disulfide linkages,[78,79] but introducing new electrostatic interactions, including HBs, to stabilize proteins is less common.[80−86] The HeX-B from the unnatural ^{mX}Tyr is distinct from the multitude of interactions engineered into T4L in that both stability and function can be enhanced noncovalently through addition of a single halogen atom.

There are many applications in which halogens can be placed adjacent to HB donor substituents, such that an HeX-B can be formed. In this particular study, the HB donor is an OH group, which can rotate to either interact with the halogen or not. An NH_2 in this position, however, would always result in an HB enhancing the XB donor capabilities of the halogen. For small molecules used in the design of protein inhibitors, or for crystal engineering or supramolecular assemblies, the types of HB donors that can facilitate formation of the HeX-B grow beyond the simple OH, NH_2, and SH substituents, including potentially cationic HB donors (which would be expected to have an even stronger polarization effect). Thus, with the HeX-B, we have now expanded the energetic and geometric properties of XBs, making this noncanonical interaction an even more powerful tool for molecular design in biomolecular engineering, medicinal chemistry, and material science.

■ ASSOCIATED CONTENT

Supporting Information

The Supporting Information is available free of charge on the ACS Publications website at DOI: 10.1021/acs.biochem.8b00603.

Table of crystallographic parameters and refinement statistics for all constructs (Table S1), tables of molecular distances around the Y18 residue of the ^{mX}Y18-T4L structures (Tables S2−S5), omit difference (F_o − F_c) electron density maps for the halogenated amino acid residues (Figure S1), figures for solvent interactions around the Y18 residue of the ^{mBr}Y18-T4L and ^{mI}Y18-T4L structures (Figures S2 and S3, respectively), plot of ΔC_p versus the hydrophobic solvent accessible surface area (Figure S4), and plot of percent activity versus stabilities of halogenated constructs relative to WT* of T4L (Figure S5) (PDF)

■ AUTHOR INFORMATION

Corresponding Author

*E-mail: Shing.Ho@ColoState.edu. Phone: (970) 491-0569.

DOI: 10.1021/acs.biochem.8b00603
Biochemistry 2018, 57, 4135−4147

ORCID

Melissa Coates Ford: 0000-0002-0253-5389
Ryan A. Mehl: 0000-0003-2932-4941
P. Shing Ho: 0000-0002-8082-4311

Funding

This work was supported by grants from the National Science Foundation (CHE-1608146) to P.S.H. and National Institutes of Health Grant GM114653A to R.A.M. A.-C.C.C. was supported by fellowships from the Wenner-Gren Foundations, Helge Ax:son Johnsons Stiftelse, Richard Dahlboms Stiftelse, and Stiftelsen Olle Engkvist Byggmästare.

Notes

The authors declare no competing financial interest.

■ ACKNOWLEDGMENTS

The authors thank Prof. R. J. Woody for his helpful discussions and reading of the manuscript.

■ REFERENCES

(1) The, M. J. (1989) Human insulin: DNA technology's first drug. *Am. J. Hosp. Pharm. 46*, S9−11.

(2) Molitch, M. E., Clemmons, D. R., Malozowski, S., Merriam, G. R., Shalet, S. M., and Vance, M. L. (2006) Evaluation and treatment of adult growth hormone deficiency: An Endocrine Society clinical practice guideline. *J. Clin. Endocrinol. Metab. 91*, 1621−1634.

(3) Paolicelli, D., Direnzo, V., and Trojano, M. (2009) Review of interferon beta-1b in the treatment of early and relapsing multiple sclerosis. *Biol.: Targets Ther. 3*, 369−376.

(4) Liu, S., Ren, J., Hong, Z., Yan, D., Gu, G., Han, G., Wang, G., Ren, H., Chen, J., and Li, J. (2013) Efficacy of erythropoietin combined with enteral nutrition for the treatment of anemia in Crohn's disease: a prospective cohort study. *Nutr. Clin. Pract. 28*, 120−127.

(5) Frokjaer, S., and Otzen, D. E. (2005) Protein drug stability: a formulation challenge. *Nat. Rev. Drug Discovery 4*, 298−306.

(6) O'Fagain, C. (2011) Engineering protein stability. *Methods Mol. Biol. 681*, 103−136.

(7) Baker, E. G., Williams, C., Hudson, K. L., Bartlett, G. J., Heal, J. W., Porter Goff, K. L., Sessions, R. B., Crump, M. P., and Woolfson, D. N. (2017) Engineering protein stability with atomic precision in a monomeric miniprotein. *Nat. Chem. Biol. 13*, 764−770.

(8) Asial, I., Cheng, Y. X., Engman, H., Dollhopf, M., Wu, B., Nordlund, P., and Cornvik, T. (2013) Engineering protein thermostability using a generic activity-independent biophysical screen inside the cell. *Nat. Commun. 4*, 2901.

(9) Gauthier, M. A., and Klok, H. A. (2008) Peptide/protein-polymer conjugates: synthetic strategies and design concepts. *Chem. Commun. (Cambridge, U. K.)*, 2591−2611.

(10) Serrano, L., Day, A. G., and Fersht, A. R. (1993) Step-wise mutation of barnase to binase. A procedure for engineering increased stability of proteins and an experimental analysis of the evolution of protein stability. *J. Mol. Biol. 233*, 305−312.

(11) Grimsley, G. R., Shaw, K. L., Fee, L. R., Alston, R. W., Huyghues-Despointes, B. M., Thurlkill, R. L., Scholtz, J. M., and Pace, C. N. (1999) Increasing protein stability by altering long-range coulombic interactions. *Protein Sci. 8*, 1843−1849.

(12) Nicholson, H., Anderson, D. E., Dao-pin, S., and Matthews, B. W. (1991) Analysis of the interaction between charged side chains and the alpha-helix dipole using designed thermostable mutants of phage T4 lysozyme. *Biochemistry 30*, 9816−9828.

(13) Wang, L., Xie, J., and Schultz, P. G. (2006) Expanding the Genetic Code. *Annu. Rev. Biophys. Biomol. Struct. 35*, 225−249.

(14) Desiraju, G. R., Ho, P. S., Kloo, L., Legon, A. C., Marquardt, R., Metrangolo, P., Politzer, P., Resnati, G., and Rissanen, K. (2013) Definition of the halogen bond (IUPAC Recommendations 2013). *Pure Appl. Chem. 85*, 1711−1713.

(15) Wang, C. W., Danovich, D., Mo, Y. R., and Shaik, S. (2014) On The Nature of the Halogen Bond. *J. Chem. Theory Comput. 10*, 3726−3737.

(16) Rosokha, S. V., Neretin, I. S., Rosokha, T. Y., Hecht, J., and Kochi, J. K. (2006) Charge-transfer character of halogen bonding: Molecular structures and electronic spectroscopy of carbon tetrabromide and bromoform complexes with organic sigma- and pi-donors. *Heteroat. Chem. 17*, 449−459.

(17) Rezac, J., and de la Lande, A. (2017) On the role of charge transfer in halogen bonding. *Phys. Chem. Chem. Phys. 19*, 791−803.

(18) Clark, T., Hennemann, M., Murray, J. S., and Politzer, P. (2007) Halogen bonding: the sigma-hole. Proceedings of "Modeling interactions in biomolecules II", Prague, September 5th-9th, 2005. *J. Mol. Model. 13*, 291−296.

(19) Nelyubina, Y. V., Antipin, M. Y., Dunin, D. S., Kotov, V. Y., and Lyssenko, K. A. (2010) Unexpected "amphoteric" character of the halogen bond: the charge density study of the co-crystal of N-methylpyrazine iodide with I-2. *Chem. Commun. 46*, 5325−5327.

(20) Scholfield, M. R., Zanden, C. M., Carter, M., and Ho, P. S. (2013) Halogen bonding (X-bonding): a biological perspective. *Protein Sci. 22*, 139−152.

(21) Brammer, L., Bruton, E. A., and Sherwood, P. (2001) Understanding the behavior of halogens as hydrogen bond acceptors. *Cryst. Growth Des. 1*, 277−290.

(22) Aakeröy, C., Desper, J., Helfrich, B. A., Metrangolo, P., Pilati, T., Resnati, G., and Stevenazzi, A. (2007) Combining halogen bonds and hydrogen bonds in the modular assembly of heteromeric infinite 1-D chains. *Chem. Commun.*, 4236−4238.

(23) Auffinger, P., Hays, F. A., Westhof, E., and Ho, P. S. (2004) Halogen bonds in biological molecules. *Proc. Natl. Acad. Sci. U. S. A. 101*, 16789−16794.

(24) Voth, A. R., Hays, F. A., and Ho, P. S. (2007) Directing macromolecular conformation by halogen bonds. *Proc. Natl. Acad. Sci. U. S. A. 104*, 6188−6193.

(25) Carter, M., Voth, A. R., Scholfield, M. R., Rummel, B., Sowers, L. C., and Ho, P. S. (2013) Enthalpy-Entropy Compensation in Biomolecular Halogen Bonds Measured in DNA Junctions. *Biochemistry 52*, 4891−4903.

(26) Ford, M. C., Saxton, M., and Ho, P. S. (2017) Sulfur as an Acceptor to Bromine in Biomolecular Halogen Bonds. *J. Phys. Chem. Lett. 8*, 4246−4252.

(27) Zhou, P., Tian, F., Zou, J., and Shang, Z. (2010) Rediscovery of Halogen Bonds in Protein-Ligand Complexes. *Mini-Rev. Med. Chem. 10*, 309−314.

(28) Wilcken, R., Zimmermann, M. O., Lange, A., Joerger, A. C., and Boeckler, F. M. (2013) Principles and Applications of Halogen Bonding in Medicinal Chemistry and Chemical Biology. *J. Med. Chem. 56*, 1363−1388.

(29) Ford, M. C., and Ho, P. S. (2016) Computational Tools To Model Halogen Bonds in Medicinal Chemistry. *J. Med. Chem. 59*, 1655−1670.

(30) Ho, P. S. (2017) Halogen bonding in medicinal chemistry: from observation to prediction. *Future Med. Chem. 9*, 637−640.

(31) Cavallo, G., Metrangolo, P., Milani, R., Pilati, T., Priimagi, A., Resnati, G., and Terraneo, G. (2016) The Halogen Bond. *Chem. Rev. 116*, 2478−2601.

(32) Scholfield, M. R., Ford, M. C., Carlsson, A. C., Butta, H., Mehl, R. A., and Ho, P. S. (2017) Structure-Energy Relationships of Halogen Bonds in Proteins. *Biochemistry 56*, 2794−2802.

(33) Matthews, B. W. (1996) Structural and genetic analysis of the folding and function of T4 lysozyme. *FASEB J. 10*, 35−41.

(34) Voth, A. R., Khuu, P., Oishi, K., and Ho, P. S. (2009) Halogen bonds as orthogonal molecular interactions to hydrogen bonds. *Nat. Chem. 1*, 74−79.

(35) Ohtake, K., Yamaguchi, A., Mukai, T., Kashimura, H., Hirano, N., Haruki, M., Kohashi, S., Yamagishi, K., Murayama, K., Tomabechi, Y., Itagaki, T., Akasaka, R., Kawazoe, M., Takemoto, C., Shirouzu, M., Yokoyama, S., and Sakamoto, K. (2015) Protein stabilization utilizing a redefined codon. *Sci. Rep. 5*, 9762.

DOI: 10.1021/acs.biochem.8b00603
Biochemistry 2018, 57, 4135−4147

(36) Borozan, S. Z., and Stojanovic, S. D. (2013) Halogen bonding in complexes of proteins and non-natural amino acids. *Comput. Biol. Chem. 47*, 231−239.
(37) Voth, A. R., and Ho, P. S. (2007) The Role of Halogen Bonding in Inhibitor Recognition and Binding by Protein Kinases. *Curr. Top. Med. Chem. 7*, 1336−1348.
(38) Sirimulla, S., Bailey, J. B., Vegesna, R., and Narayan, M. (2013) Halogen Interactions in Protein-Ligand Complexes: Implications of Halogen Bonding for Rational Drug Design. *J. Chem. Inf. Model. 53*, 2781−2791.
(39) Wilcken, R., Zimmermann, M. O., Lange, A., Zahn, S., and Boeckler, F. M. (2012) Using halogen bonds to address the protein backbone: a systematic evaluation. *J. Comput.-Aided Mol. Des. 26*, 935−945.
(40) Matsumura, M., and Matthews, B. W. (1989) Control of enzyme activity by an engineered disulfide bond. *Science 243*, 792−794.
(41) Noren, C. J., Anthony-Cahill, S. J., Griffith, M. C., and Schultz, P. G. (1989) A general method for site-specific incorporation of unnatural amino acids into proteins. *Science 244*, 182−188.
(42) Hammill, J. T., Miyake-Stoner, S., Hazen, J. L., Jackson, J. C., and Mehl, R. A. (2007) Preparation of site-specifically labeled fluorinated proteins for 19F-NMR structural characterization. *Nat. Protoc. 2*, 2601−2607.
(43) Peeler, J. C., and Mehl, R. A. (2012) Site-specific incorporation of unnatural amino acids as probes for protein conformational changes. *Methods Mol. Biol. 794*, 125−134.
(44) Kabsch, W. (2010) Xds. *Acta Crystallogr., Sect. D: Biol. Crystallogr. 66*, 125−132.
(45) Winn, M. D., Ballard, C. C., Cowtan, K. D., Dodson, E. J., Emsley, P., Evans, P. R., Keegan, R. M., Krissinel, E. B., Leslie, A. G. W., McCoy, A., McNicholas, S. J., Murshudov, G. N., Pannu, N. S., Potterton, E. A., Powell, H. R., Read, R. J., Vagin, A., and Wilson, K. S. (2011) Overview of the CCP4 suite and current developments. *Acta Crystallogr., Sect. D: Biol. Crystallogr. 67*, 235−242.
(46) Adams, P. D., Afonine, P. V., Bunkoczi, G., Chen, V. B., Davis, I. W., Echols, N., Headd, J. J., Hung, L. W., Kapral, G. J., Grosse-Kunstleve, R. W., McCoy, A. J., Moriarty, N. W., Oeffner, R., Read, R. J., Richardson, D. C., Richardson, J. S., Terwilliger, T. C., and Zwart, P. H. (2010) PHENIX: a comprehensive Python-based system for macromolecular structure solution. *Acta Crystallogr., Sect. D: Biol. Crystallogr. 66*, 213−221.
(47) Heinz, D. W., Baase, W. A., and Matthews, B. W. (1992) Folding and Function of a T4 Lysozyme Containing 10 Consecutive Alanines Illustrate the Redundancy of Information in an Amino-Acid-Sequence. *Proc. Natl. Acad. Sci. U. S. A. 89*, 3751−3755.
(48) Frisch, M. J., Trucks, G. W., Schlegel, H. B., Scuseria, G. E., Robb, M. A., Cheeseman, J. R., Montgomery, J. A., Jr., Vreven, T., Kudin, K. N., Burant, J. C., Millam, J. M., Iyengar, S. S., Tomasi, J., Barone, V., Mennucci, B., Cossi, M., Scalmani, G., Rega, N., Petersson, G. A., Nakatsuji, H., Hada, M., Ehara, M., Toyota, K., Fukuda, R., Hasegawa, J., Ishida, M., Nakajima, T., Honda, Y., Kitao, O., Nakai, H., Klene, M., Li, X., Knox, J. E., Hratchian, H. P., Cross, J. B., Bakken, V., Adamo, C., Jaramillo, J., Gomperts, R., Stratmann, R. E., Yazyev, O., Austin, A. J., Cammi, R., Pomelli, C., Ochterski, J. W., Ayala, P. Y., Morokuma, K., Voth, G. A., Salvador, P., Dannenberg, J. J., Zakrzewski, V. G., Dapprich, S., Daniels, A. D., Strain, M. C., Farkas, O., Malick, D. K., Rabuck, A. D., Raghavachari, K., Foresman, J. B., Ortiz, J. V., Cui, Q., Baboul, A. G., Clifford, S., Cioslowski, J., Stefanov, B. B., Liu, G., Liashenko, A., Piskorz, P., Komaromi, I., Martin, R. L., Fox, D. J., Keith, T., Al-Laham, M. A., Peng, C. Y., Nanayakkara, A., Challacombe, M., Gill, P. M. W., Johnson, B., Chen, W., Wong, M. W., Gonzalez, C., and Pople, J. A. (2004) *Gaussian 03*, revision C.02, Gaussian, Inc., Wallingford, CT.
(49) Zhou, H. X., and Pang, X. (2018) Electrostatic Interactions in Protein Structure, Folding, Binding, and Condensation. *Chem. Rev. 118*, 1691−1741.
(50) Boys, S. F., and Bernardi, F. (1970) Calculation of Small Molecular Interactions by Differences of Separate Total Energies - Some Procedures with Reduced Errors. *Mol. Phys. 19*, 553.
(51) Peterson, K. A., Shepler, B. C., Figgen, D., and Stoll, H. (2006) On the spectroscopic and thermochemical properties of ClO, BrO, IO, and their anions. *J. Phys. Chem. A 110*, 13877−13883.
(52) Carter, M., Rappe, A. K., and Ho, P. S. (2012) Scalable Anisotroplic Shape and Electrostatic Models for Biological Bromine Halogen Bonds. *J. Chem. Theory Comput. 8*, 2461−2473.
(53) Vander Zanden, C. M., Carter, M., and Ho, P. S. (2013) Determining thermodynamic properties of molecular interactions from single crystal studies. *Methods 64*, 12−18.
(54) Scholfield, M. R., Ford, M. C., Vander Zanden, C. M., Billman, M. M., Ho, P. S., and Rappe, A. K. (2015) Force Field Model of Periodic Trends in Biomolecular Halogen Bonds. *J. Phys. Chem. B 119*, 9140−9149.
(55) Gorin, G., Wang, S. F., and Papapavlou, L. (1971) Assay of Lysozyme by Its Lytic Action on M-Lysodeikticus Cells. *Anal. Biochem. 39*, 113−127.
(56) Kuroki, R., Weaver, L. H., and Matthews, B. W. (1995) Structure-Based Design of a Lysozyme with Altered Catalytic Activity. *Nat. Struct. Mol. Biol. 2*, 1007−1011.
(57) Matthews, B. W. (1993) Structural and genetic analysis of protein stability. *Annu. Rev. Biochem. 62*, 139−160.
(58) Vallejos, M., Auffinger, P., and Ho, P. (2012) Halogen interactions in biomolecular crystal structures. In *International Tables of Crystallography, Volume F* (Himmel, D. M., Ed.) Chapter 23.26, International Union of Crystallography.
(59) Matsumura, M., Wozniak, J. A., Sun, D. P., and Matthews, B. W. (1989) Structural studies of mutants of T4 lysozyme that alter hydrophobic stabilization. *J. Biol. Chem. 264*, 16059−16066.
(60) Hawkes, R., Grutter, M. G., and Schellman, J. (1984) Thermodynamic stability and point mutations of bacteriophage T4 lysozyme. *J. Mol. Biol. 175*, 195−212.
(61) Sturtevant, J. M. (1977) Heat capacity and entropy changes in processes involving proteins. *Proc. Natl. Acad. Sci. U. S. A. 74*, 2236−2240.
(62) Privalov, P. L., and Gill, S. J. (1988) Stability of Protein-Structure and Hydrophobic Interaction. *Adv. Protein Chem. 39*, 191−234.
(63) Privalov, P. L., and Makhatadze, G. I. (1992) Contribution of hydration and non-covalent interactions to the heat capacity effect on protein unfolding. *J. Mol. Biol. 224*, 715−723.
(64) Spolar, R. S., Ha, J. H., and Record, M. T., Jr (1989) Hydrophobic effect in protein folding and other noncovalent processes involving proteins. *Proc. Natl. Acad. Sci. U. S. A. 86*, 8382−8385.
(65) Myers, J. K., Pace, C. N., and Scholtz, J. M. (1995) Denaturant m values and heat capacity changes: relation to changes in accessible surface areas of protein unfolding. *Protein Sci. 4*, 2138−2148.
(66) Makhatadze, G. I., and Privalov, P. L. (1995) Energetics of protein structure. *Adv. Protein Chem. 47*, 307−425.
(67) El Hage, K., Pandyarajan, V., Phillips, N. B., Smith, B. J., Menting, J. G., Whittaker, J., Lawrence, M. C., Meuwly, M., and Weiss, M. A. (2016) Extending Halogen-based Medicinal Chemistry to Proteins: IODO-INSULIN AS A CASE STUDY. *J. Biol. Chem. 291*, 27023−27041.
(68) Abraham, M. H., Abraham, R. J., Aliev, A. E., and Tormena, C. F. (2015) Is there an intramolecular hydrogen bond in 2-halophenols? A theoretical and spectroscopic investigation. *Phys. Chem. Chem. Phys. 17*, 25151−25159.
(69) Lee, C., Park, S.-H., Lee, M.-Y., and Yu, M.-H. (2000) Regulation of protein function by native metastability. *Proc. Natl. Acad. Sci. U. S. A. 97*, 7727−7731.
(70) Danelius, E., Andersson, H., Jarvoll, P., Lood, K., Grafenstein, J., and Erdelyi, M. (2017) Halogen Bonding: A Powerful Tool for Modulation of Peptide Conformation. *Biochemistry 56*, 3265−3272.

DOI: 10.1021/acs.biochem.8b00603
Biochemistry 2018, 57, 4135−4147

(71) Bissantz, C., Kuhn, B., and Stahl, M. (2010) A Medicinal Chemist's Guide to Molecular Interactions. *J. Med. Chem. 53*, 5061−5084.
(72) Hunter, C. A. (2004) Quantifying intermolecular interactions: guidelines for the molecular recognition toolbox. *Angew. Chem., Int. Ed. 43*, 5310−5324.
(73) Richter, F., Leaver-Fay, A., Khare, S. D., Bjelic, S., and Baker, D. (2011) De novo enzyme design using Rosetta3. *PLoS One 6*, e19230.
(74) Rowe, R. K., and Ho, P. S. (2017) Relationships between hydrogen bonds and halogen bonds in biological systems. *Acta Crystallogr., Sect. B: Struct. Sci., Cryst. Eng. Mater. 73*, 255−264.
(75) Sheu, S. Y., Yang, D. Y., Selzle, H. L., and Schlag, E. W. (2003) Energetics of hydrogen bonds in peptides. *Proc. Natl. Acad. Sci. U. S. A. 100*, 12683−12687.
(76) Baase, W. A., Liu, L., Tronrud, D. E., and Matthews, B. W. (2010) Lessons from the lysozyme of phage T4. *Protein Sci. 19*, 631−641.
(77) Lyu, P. C., Sherman, J. C., Chen, A., and Kallenbach, N. R. (1991) Alpha-helix stabilization by natural and unnatural amino acids with alkyl side chains. *Proc. Natl. Acad. Sci. U. S. A. 88*, 5317−5320.
(78) Hegazy, U. M., and Mannervik, B. (2007) Enhancement of enzyme efficiency and stability by incorporation of unnatural amino acid residues in a targeted functional site. *FASEB J. 21*, A1012−A1012a.
(79) Liu, T., Wang, Y., Luo, X., Li, J., Reed, S. A., Xiao, H., Young, T. S., and Schultz, P. G. (2016) Enhancing protein stability with extended disulfide bonds. *Proc. Natl. Acad. Sci. U. S. A. 113*, 5910−5915.
(80) Loladze, V. V., Ibarra-Molero, B., Sanchez-Ruiz, J. M., and Makhatadze, G. I. (1999) Engineering a thermostable protein via optimization of charge-charge interactions on the protein surface. *Biochemistry 38*, 16419−16423.
(81) Trejo, F., Gelpi, J. L., Ferrer, A., Boronat, A., Busquets, M., and Cortes, A. (2001) Contribution of engineered electrostatic interactions to the stability of cytosolic malate dehydrogenase. *Protein Eng., Des. Sel. 14*, 911−917.
(82) Makhatadze, G. I., Loladze, V. V., Gribenko, A. V., and Lopez, M. M. (2004) Mechanism of thermostabilization in a designed cold shock protein with optimized surface electrostatic interactions. *J. Mol. Biol. 336*, 929−942.
(83) Tigerstrom, A., Schwarz, F., Karlsson, G., Okvist, M., Alvarez-Rua, C., Maeder, D., Robb, F. T., and Sjolin, L. (2004) Effects of a novel disulfide bond and engineered electrostatic interactions on the thermostability of azurin. *Biochemistry 43*, 12563−12574.
(84) Gribenko, A. V., Patel, M. M., Liu, J., McCallum, S. A., Wang, C., and Makhatadze, G. I. (2009) Rational stabilization of enzymes by computational redesign of surface charge-charge interactions. *Proc. Natl. Acad. Sci. U. S. A. 106*, 2601−2606.
(85) Sokalingam, S., Raghunathan, G., Soundrarajan, N., and Lee, S. G. (2012) A study on the effect of surface lysine to arginine mutagenesis on protein stability and structure using green fluorescent protein. *PLoS One 7*, e40410.
(86) Raghunathan, G., Sokalingam, S., Soundrarajan, N., Madan, B., Munussami, G., and Lee, S. G. (2013) Modulation of protein stability and aggregation properties by surface charge engineering. *Mol. BioSyst. 9*, 2379−2389.
(87) *The PyMOL Molecular Graphics System*, version 1.8 (2015) Schrödinger, LLC.
(88) van Holde, K., Johnson, W. C., and Ho, P. S. (2006) *Principles of Physical Biochemistry*, 2nd ed., Pearson Prentice Hall, Upper Saddle River, NJ.
(89) Bondi, A. (1964) van der Waals volumes and radii. *J. Phys. Chem. 68*, 441−451.

DOI: 10.1021/acs.biochem.8b00603
Biochemistry 2018, 57, 4135−4147